A Statistical Study of Large-Scale, Long-Period Variability in North Pacific Sea Surface Temperature Anomalies

JOEL MICHAELSEN[1]

Department of Geography, University of California, Berkeley, 94720

(Manuscript received 20 February 1981, in final form 15 March 1982)

ABSTRACT

Frequency domain principal components analysis, a technique which involves extracting the eigenvalues and eigenvectors of the cross spectrum of a multivariate time series, is used to analyze the development and movement of sea surface temperature (SST) anomalies in the North Pacific. A prominent feature of the low-frequency SST field is an oscillatory pattern with a return period of about four to seven years. It involves the slow migration of an anomaly northward into the western North Pacific where the anomaly undergoes rapid expansion and intensification and then begins to deteriorate as it moves eastward. It is suggested that the rapid expansion in midlatitudes is caused by a positive feedback between the SST anomalies, the atmospheric long waves, and cyclonic short waves.

1. Introduction

The existence of large-scale, low frequency sea surface temperature (SST) anomalies in the North Pacific has been well documented (cf. Namias, 1969, 1970). There are indications that these anomalies may retain their coherence long enough to be advected around the North Pacific gyre. Namias (1970) noted high lag correlations between the northern (35–55°N) and southern (20–35°N) regions when the southern region lagged by as much as two years, and he suggested advection through the gyre as a possible mechanism. Namias (1959) and Favorite and McLain (1974) described a case during the 1955–59 period when an SST anomaly drifted eastward across the midlatitude North Pacific. Favorite and McLain hypothesized a continuous cycling of SST anomalies around the North Pacific gyre causing anomalies to reappear in a given location every five to six years. Davis (1976) has produced evidence of eastward movement of large SST anomalies in the western midlatitude North Pacific from a statistical model of air–sea interactions.

In order to describe the variability of an SST anomaly field one is faced with a problem in two spatial dimensions and time. An approach which has been applied to this problem has been to treat the spatial dimensions as multi-variate time series and to isolate large-scale variability patterns with spatial empirical orthogonal functions, or principal components (Davis, 1976; Weare *et al.*, 1976). This procedure does not explicitly retain information on the spatial distribution of the individual variables (grid points) in the same way as would a multi-dimensional space–time series analysis. The requirement that the principal components contain maximum amounts of the total variance of the SST fields does insure that coherent large-scale anomaly patterns are produced, however, at least in the first few principal components.

A more serious shortcoming of this approach is the fact that only instantaneous temporal covariance is resolved by the principal components. Thus, anomalies which move in space over time cannot be fully identified. In addition, there is no explicit differentiation between patterns on different time scales.

A technique which remedies these two shortcomings of standard principal components (SPC) is frequency domain principal components analysis (FDPC). This technique involves extracting the eigenvectors and eigenvalues of the cross spectrum matrix of a multi-variate time series, rather than those of the covariance matrix. Theoretical developments of FDPC can be found in Brillinger (1975) or Wallace and Dickinson (1972), while applications include analysis of long European temperature series (Brillinger, 1975) and of tropical wave disturbances (Wallace, 1972).

The general relationship between SPC and FDPC can be understood by considering that the spectral density of a vector-valued stationary time-series $\mathbf{X}(t)$ is defined as

$$\mathbf{f}_{\mathbf{X}}(\lambda) = \sum_{u=-\infty}^{\infty} \mathbf{c}(u)e^{-iu\lambda},$$

where $\mathbf{c}(u) = E[(\mathbf{X}(t+u), \mathbf{X}(t)]$ is the cross-covariance matrix, while the covariance matrix analyzed in SPC is simply $\mathbf{c}(0) = E[\mathbf{X}(t), \mathbf{X}(t)]$. In addition, the power spectrum provides for the separa-

[1] Present affiliation: Department of Geography, University of California, Santa Barbara, CA 93106.

0022-3670/82/070694-10$06.50

tion of patterns with different time-scales by partitioning the variance by frequency. Intuitively, FDPC provides an increase in information over SPC analogous to the increase in cross-spectrum analysis over bi-variate correlation analysis. Thus, FDPC should prove a more useful descriptive procedure in an SST anomaly field where slow advection of anomalies implies that different points in space will have cross-spectra with significant coherence in low frequencies at non-zero phase lags.

In this paper 30 years of North Pacific SST anomalies are analyzed using FDPC techniques in an attempt to identify and describe the development of long period (longer than one year) SST anomalies. The information provided by the FDPC analysis should indicate to what extent anomalies do retain their coherence as they drift around the North Pacific gyre.

2. Theory

The following theoretical development is from Brillinger (1975, p. 344). Suppose $\mathbf{X}(t)$ is an r vector-valued second-order stationary time series with mean 0, absolutely summable covariance function $\mathbf{cx}(u)$, and spectral density matrix $\mathbf{fx}(\lambda)$. $\mathbf{fx}(\lambda)$ is an $r \times r$ non-negative definite hermitian matrix and so has r real non-negative eigenvalues, $m_k(\lambda)$, associated with r complex orthogonal eigenvectors, $\mathbf{V}_k(\lambda)$. By convention the $m_k(\lambda)$ are ordered so that $m_1(\lambda) \geqslant \cdots \geqslant m_r(\lambda)$.

Define the $q \times r$, $q < r$, matrix $\mathbf{B}(\lambda)$ by

$$\mathbf{B}(\lambda) = \begin{bmatrix} \overline{\mathbf{V}_1(\lambda)^T} \\ \vdots \\ \overline{\mathbf{V}_q(\lambda)^T} \end{bmatrix} \tag{1}$$

and the $r \times q$ matrix $\mathbf{C}(\lambda)$ by

$$\mathbf{C}(\lambda) = (\mathbf{V}_1(\lambda), \cdots, \mathbf{V}_q(\lambda)) = \overline{\mathbf{B}(\lambda)^T}, \tag{2}$$

where the symbol $\overline{(\ )^T}$ indicates the hermitian transpose. Then the q vector valued principal component series

$$\mathbf{Y}(t) = \sum_u \mathbf{b}(t-u)\mathbf{X}(t), \tag{3}$$

where

$$\mathbf{b}(u) = (2\pi)^{-1} \int_0^{2\pi} \mathbf{B}(\alpha) \exp(i\alpha u) d\alpha \tag{4}$$

minimizes the quantity

$$E\{[\mathbf{X}(t) - \sum_u \mathbf{c}(t-u)\mathbf{Y}(t)]^T \times [\mathbf{X}(t) - \sum_u \mathbf{c}(t-u)\mathbf{Y}(t)]\}, \tag{5}$$

where

$$\mathbf{c}(u) = (2\pi)^{-1} \int_0^{2\pi} \mathbf{C}(\alpha) \exp(i\alpha u) d\alpha. \tag{6}$$

The minimum obtained is $\int_0^{2\pi} \sum_{k>q} [m_k(\alpha)] d\alpha$.

Now, if $\mathbf{X}(t)$ has a Cramér representation (Brillinger, 1975, p. 100)

$$\mathbf{X}(t) = \int_0^{2\pi} \exp(i\alpha t) d\mathbf{Z}x(\alpha) \quad t = 0, \pm 1, \ldots, \tag{7}$$

then

$$\mathbf{Y}(t) = \int_0^{2\pi} \mathbf{B}(\alpha) \exp(i\alpha t) d\mathbf{Z}x(\alpha), \tag{8}$$

and the kth principal component series is given by

$$Y_k(t) = \int_0^{2\pi} \overline{\mathbf{V}_k(\alpha)^T} \exp(i\alpha t) d\mathbf{Z}x(\alpha). \tag{9}$$

The principal component series has a spectral density matrix

$$\begin{aligned} fy_k y_j(\lambda) &= m_k(\lambda), \quad k = j \\ &\to 0 \quad , \quad k \neq j. \end{aligned} \tag{10}$$

The cross spectrum between $\mathbf{X}_j(t)$ and $\mathbf{Y}_k(t)$ is given by

$$fy_k x_j(\lambda) = m_k(\lambda)\overline{V_{kj}(\lambda)}, \tag{11}$$

with phase spectrum

$$P_{kj(\lambda)} = \arg(\overline{V_{kj}(\lambda)}), \tag{12}$$

coherence square

$$R_{kj}(\lambda) = m_k(\lambda)|V_{kj}(\lambda)|^2 / fx_j(\lambda), \tag{13}$$

and gain

$$G_{kj}(\lambda) = |V_{kj}(\lambda)|. \tag{14}$$

It should be noted that the $\mathbf{V}_k(\lambda)$ are only unique up to a constant multiplier of modulus 1. Thus it is necessary to specify one series $X_j(t)$ which have phase of 0 with $Y_k(t)$ at all frequencies. In this study the grid 45N/155E was arbitrarily chosen for this role.

3. Data and computational procedures

The SST data were taken from a set developed by Dr. Namias and others at Scripps Institute. It consists of monthly averages for the period 1947–76 from more than 150 5° squares in the North Pacific between 20 and 55°N. 32 sites at 5° intervals of latitude and 10° intervals of longitude between 30 and 45°N latitude and 165°E and 135°W longitude were selected for this study (see Fig. 1). Closer spacing was used in the north–south directions after preliminary analysis indicated that the drop-off in coherence was roughly twice as rapid as in the east–west direction. The data contained a trivial number of missing values (no more than three in any one series) which were filled by linear interpolation from neighboring values in time.

To identify anomaly patterns, the periodic annual

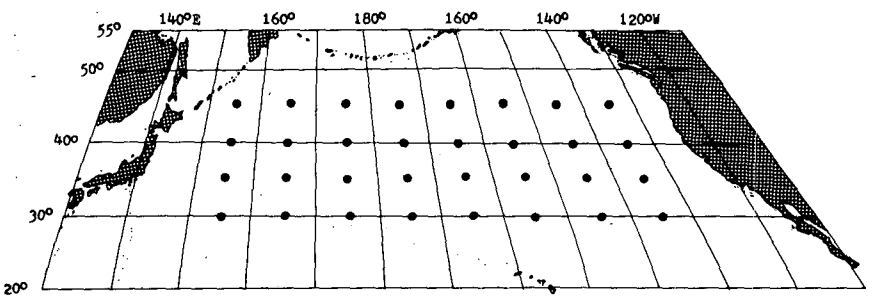

FIG. 1. SST grid points used in this study.

cycle was removed by subtracting the 30-year monthly averages from the individual monthly values. The assumption implicit in this step is that there is no interaction between the annual cycle and the anomaly patterns—that they are not seasonally dependent. This seems a reasonable assumption as a first approximation for the low frequency range, $\lambda < {}^{1}/_{12}$ cpm (cycles per month). Linear trends representing a first order non-stationary were also removed.

The cross-spectra were calculated by the direct method of smoothing the periodigrams. In the interest of stability of the estimates, a bandwidth of 0.02 cpm was used, so each spectral estimate had 16 degrees of freedom. The use of a relatively wide bandwidth increases the danger of bias, so the series were tapered and pre-whitened prior to transforming (Jenkins and Watts, 1968). Most of the series showed evidence of first-order autoregressive components

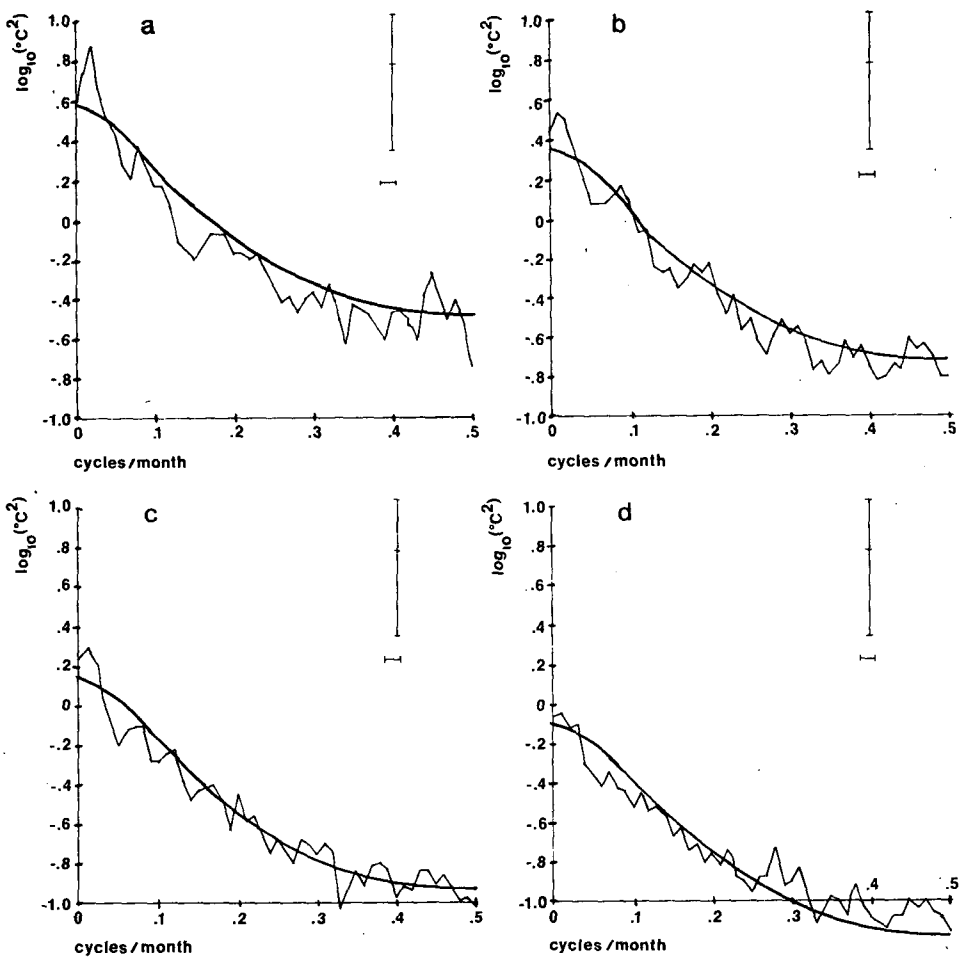

FIG. 2. Power spectra, $m_k(\lambda)$, of the first four FDPC of SST anomaly field: (a) $k = 1$, (b) $k = 2$, (c) $k = 3$, (d) $k = 4$. Smooth curves represent spectra of a first-order autoregressive process with coefficient 0.55. Vertical bars give approximate 0.95 confidence intervals for the theoretical spectra; horizontal bars give the bandwidth.

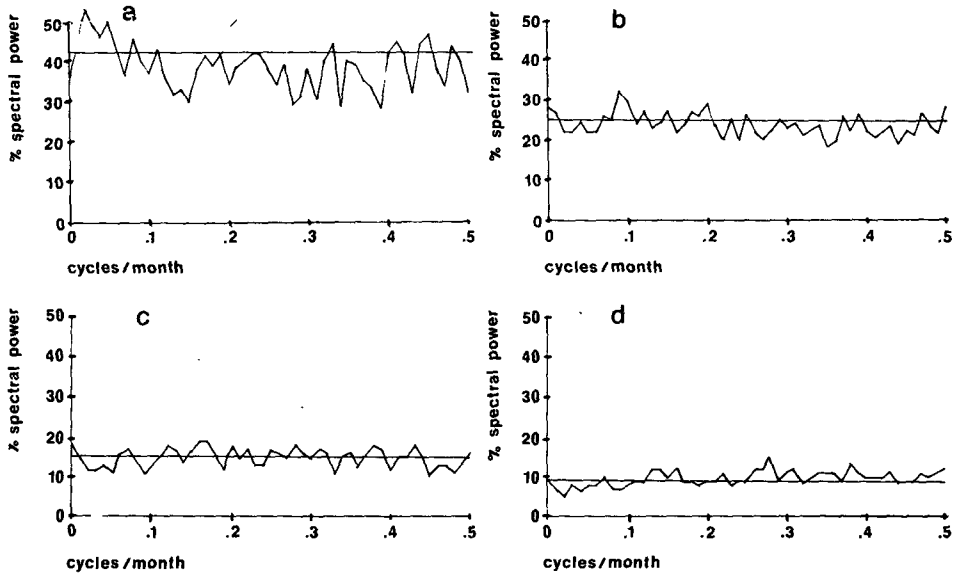

FIG. 3. Percent of cross-spectral amplitude contained in each FDPC by frequency. (a) $k = 1$, (b) $k = 2$, (c) $k = 3$, (d) $k = 4$.

with coefficients ranging between 0.3 and 0.7. It is a good practice to use the same filter for all series to retain phase and coherency relationships, therefore the average of all the first order coefficients, 0.55, was used to pre-whiten all the series. The spectra were post-darkened by applying the frequency response of the filter to the spectral estimates. Eigenvalues and eigenvectors of the cross-spectrum matrix were extracted using a standard iterative routine.

4. Results

The power spectra, $m_k(\lambda)$, $k = 1, 4$, of the most important frequency domain principal components are shown in Fig. 2. The smooth curves are the theoretical spectra of first-order autoregressive processes with lag-one correlation of 0.55. In general the components fit the model, especially the second and third FDPC's. In this respect the frequency domain components are like the principal time domain components of Davis (1976). There is a slight, but systematic, decrease in autoregressiveness in the lower components. The only significant deviations from red noise are the 0.02 cpm band of the first component (which is outside the approximate 0.95 confidence interval for the process), and the high frequency range of the fourth component (which is systematically above the expected power). The latter would probably fit an autoregressive model with a lower lag-one correlation.

The graphs in Fig. 3 give the percent of the cross-spectral amplitude contained in each FDPC by frequency. The horizontal dashed lines show the percent of variance over all frequencies contained in each FDPC. The cumulative total for all four FDPC's is 89.7%. Davis obtained a total of ~50% for the first five SPC's, so the FDPC's provide a more efficient representation of the SST field, presumably due to the inclusion of lag relationships and the identification of different patterns at different frequencies.

The total spectral amplitude (i.e. the sum of the autospectral power over all grid points) is highest in

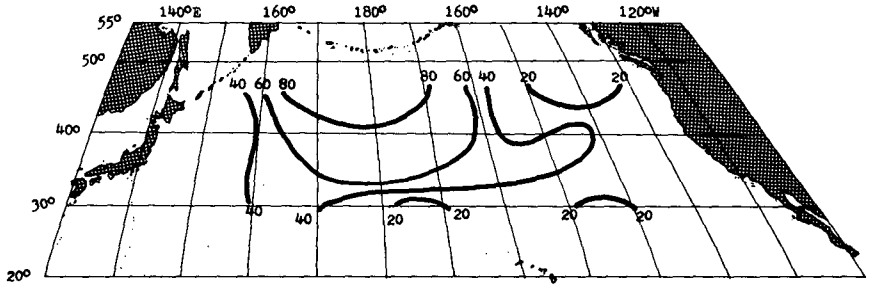

FIG. 4. Coherence square × 100 between SST grid points and first FDPC in frequency band $\lambda = 0.02$ cpm. Contour interval is 20.

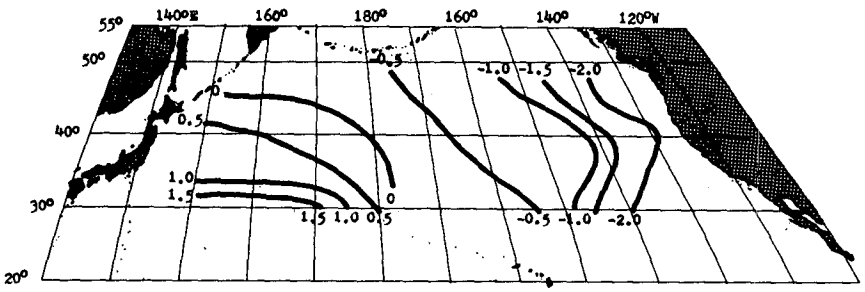

FIG. 5. Phase in radians between SST grid points and first FDPC in frequency band λ − 0.02 cpm. Negative values indicate that grid point trails FDPC which is arbitrarily assigned 0 phase with 45°N/155°E. Contour interval is 0.5 radians.

the 0.02 cpm band. The maximum percent of cross-spectral amplitude contained in a single frequency band is found in the same band of the first FDPC. Thus, the peak in the first FDPC spectrum in the 0.02 cpm band is the result of both the peak in total amplitude and the peak in percentage of total amplitude contained in the first FDPC. The variance in this band represents 12.5% of the variance of the first FDPC. This is more than three times as much as the next largest single band and as much as the whole range of frequencies higher than 0.3 cpm.

In Fig. 4 the squared factor loadings (coherence square between individual sites and the first component), R_{1j} (0.02) from (13), are mapped for the 0.02 cpm frequency band. The coherency pattern indicates that the core region of the first component at this frequency is centered in the western half of the North Pacific. This distribution is similar to that of the first time domain component in Davis (1976) which suggests the dominance of large-scale, low-frequency variations in the total variance of the SST field.

The distribution of the phase, P_{1j} (0.02) in (12), between the first component and the jth SST series at 0.02 cpm shows a very interesting pattern of movement (see Fig. 5). It appears that the SST anomalies move into the North Pacific from the southwest and then drift eastward in the midlatitudes. There is no indication of a westward return flow, although it is possible that such a process could be operating south of the study area. Anomalies move northward rather slowly out of the southwest, accelerate as they move eastward in midlatitudes, and slow down again as they approach the eastern edge of the basin.

It is not possible to estimate absolute time lags with much confidence, since the temporal resolution is poor in the low frequency range. In any case, there is probably a certain amount of variation in the phase between different oscillations, so any estimate has to be considered an average. Approximate lags can be derived by assuming that $\lambda = 0.02$ cpm is a mean frequency for the oscillation. Time lags derived under this assumption are shown in Fig. 6. The results indicate that it may take more than a year for anomalies to move northward from 30 to 45° in the western North Pacific, but they move eastward across most of the midlatitude ocean in six to eight months. Rough calculations of phase speed give results on the order of 10^{-2} m s^{-1} for the northward movement and 10^{-1} m s^{-1} for the eastward drift. This clearly rules out simple advection through the currents for the northward drift, since the observed current speeds in that sector are two orders of magnitude larger than the phase speed of the anomalies. The speed of the eastward movement is within the general range of velocities of the North Pacific current.

The differences in phase speed also imply changes in spatial scale. The anomalies expand rapidly once

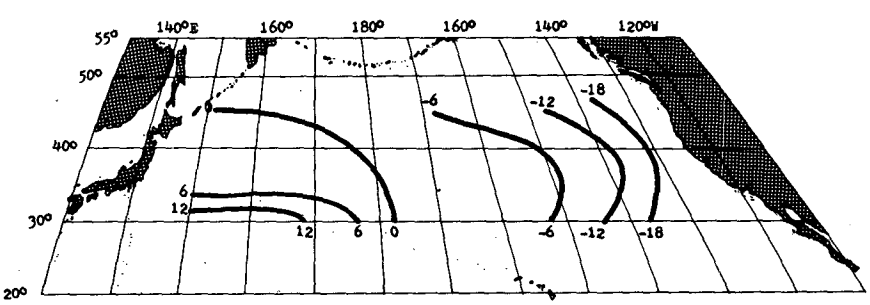

FIG. 6. Approximate phase lag in months between SST grid points and first FDPC in frequency band λ − 0.02 cpm. Negative values indicate that grid point trails FDPC. Contour interval is 6 months.

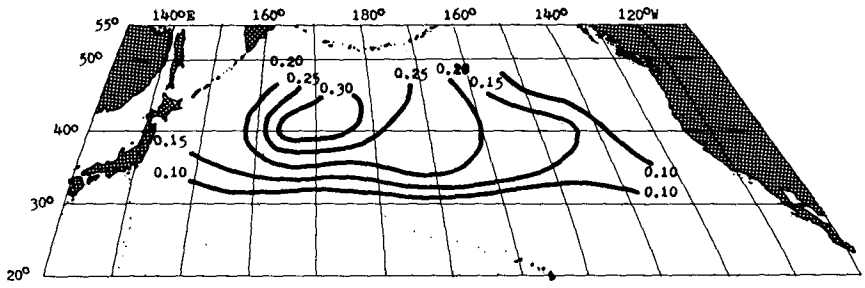

FIG. 7. Gain of SST grid points on first component in frequency band $\lambda = 0.02$. Contour intervalis is 0.05.

they reach midlatitudes and then shrink again as they approach the eastern boundary. Furthermore, they appear to increase markedly in amplitude in the western midlatitude Pacific as indicated by the distribution of the gain between individual stations and the first component, G_{1j} (0.02), from (14), in Fig. 7. The anomalies then begin decreasing in amplitude as they move toward the eastern boundary of the ocean.

These phase, coherence, and gain mappings between the first FDPC and the grid points provide a convenient tool for representing the process being studied. The determination of statistical significance for them is not possible, however, so the coherence, phase, and gain of the cross-spectra in the 0.02 cpm band between 45°N, 175°W and selected grid points along the path of the progression are presented in Fig. 8. 45°N, 175°W was selected because it has the highest coherence with the first FDPC at 0.02 cpm. The graphs tell almost the same story as the maps of the first FDPC. Significant coherence is maintained over most of the path but not all the way to the North American coast. The phase lag changes by more than 3 rad (more than two-year time lags) between 30°N, 165°E and 40°N, 145°W. The gain shows the rapid intensification of anomalies moving into midlatitudes followed by gradual weakening during the eastward trip across the midlatitude Pacific.

In summary, a fairly clear picture of the space-time behavior of these low frequency anomalies emerges. They move slowly northeastward out of the southwest corner of the study area. In about a year they become established in the midlatitude western North Pacific. Here they undergo rapid intensification and expansion and begin to drift eastward. As the eastward motion progresses over the next year or so, the anomalies tend to decrease in amplitude, shrink in size, and lose their coherency. In other words, the signal is strong in the western half of the ocean, and the anomalies do move eastward, but they do not always survive well enough to be recognizable at the eastern boundary.

It is not surprising that Davis' first SST SPC is concentrated in the region where the anomaly progression reaches its greatest extent and intensity. It is at this point that the anomalies exhibit the greatest instantaneous spatial coherence, and principal components are constructed using criteria of maximizing variance explained. Davis found that at this stage sea-level pressure seems to lead SSTs, but the evi-

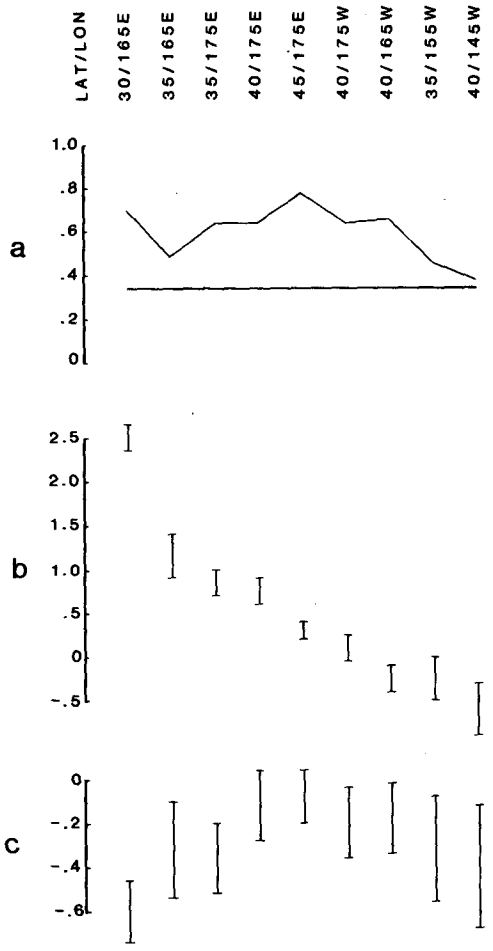

FIG. 8. Cross spectra between SST at 45°N 175°W and SST at other grid points: (a) coherence, (b) phase (negative indicates grid point lags 45°N 175°W), (c) $\log_{10}$ gain. The horizontal line in (a) is the 0.05 significance level under a null hypothesis of 0 coherence, while error bars in (b) and (c) give approximate 0.95 confidence intervals.

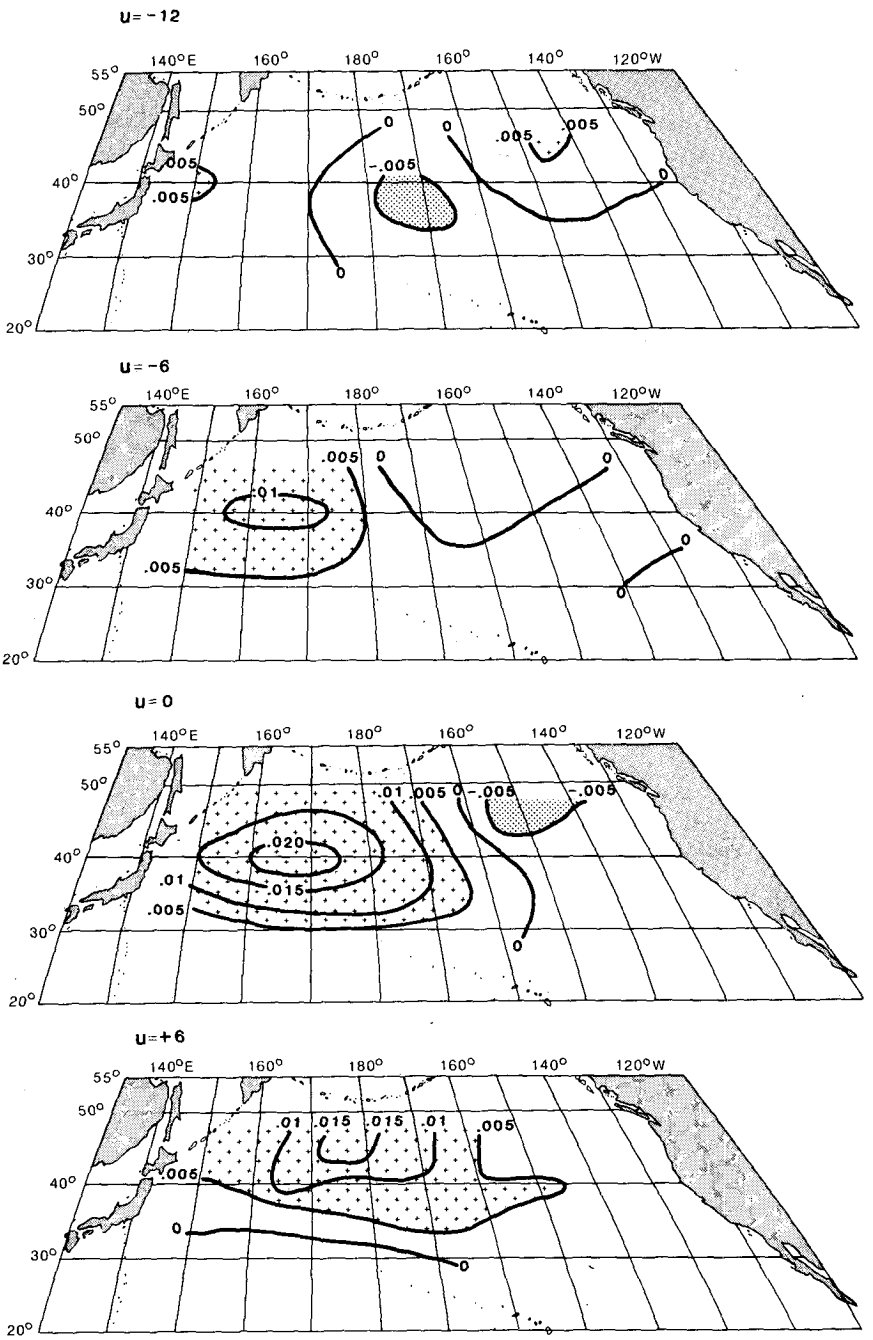

FIG. 9. Impulse response, $b(u)$, of first FDPC on SST grid points at 6-month intervals. Contour interval is 0.005 and areas greater than 0.005 or less than −0.005 are shaded.

dence in this paper indicates that the SST anomaly has already been evolving over a year, or more. Thus, it does not necessarily follow that atmospheric pressure patterns lead SST patterns, or even that the two media are coupled, throughout the full development of the SST anomaly.

The temporal behavior of the anomaly pattern can be described by the time series of the first component. In this case, however, interpretation is complicated by the inclusion of time lags. Thus, in order for a peak in the component series to occur at some time $t = t_0$, peak SST anomalies must occur in the northwest corner of the study area at $t = t_0$. In addition, peaks must have already occurred in the southwest at some earlier time $t = t_0 - \gamma$ (where $\gamma > 0$), and will occur in the mid to eastern North Pacific at some

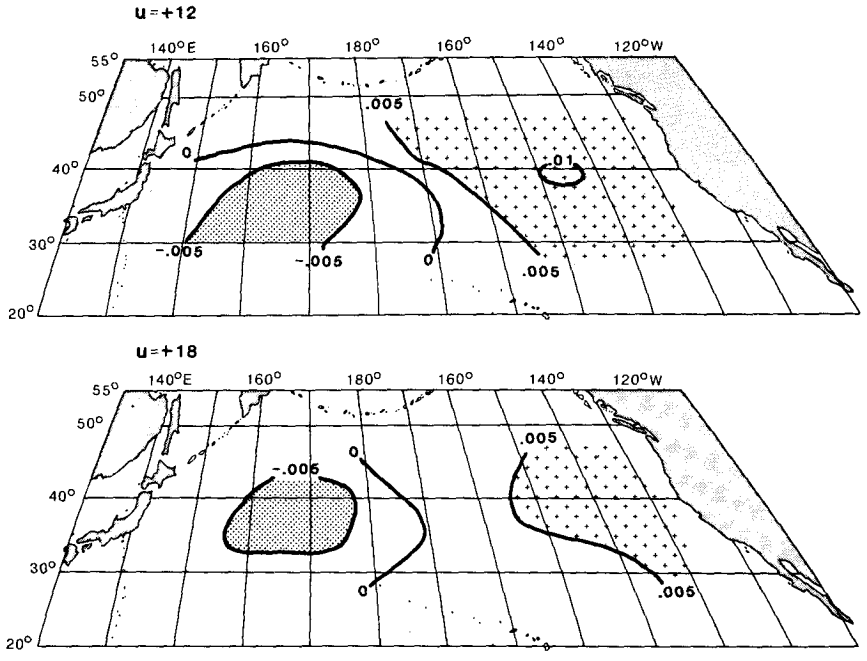

FIG. 9. (*Continued*)

future date $t = t_0 + \gamma$. The amplitude of the component series at $t = t_0$ measures not only the conformity of the current SST anomaly pattern to the prescribed pattern but also the similarity between the evolution of the SST pattern over a year or more before and after $t = t_0$ to the evolution of the prescribed pattern.

The temporal progression of spatial patterns necessary to record a high value of the first component can be seen by examining the time domain impulse response [$b(u)$ in (3)] of the transfer function of each SST series on the first component. The features described above are evident in the series of maps of the impulse responses at six month intervals (Fig. 9). When an anomaly pattern develops in a fashion similar to the impulse response function, a peak occurs in the component series contemporaneous with a peak anomaly in the northwest corner of the study area, while an anomaly of opposite sign but similar development will produce a trough in the component series.

The time series of the first component, $Y_1(t)$, with a smoothed version are graphed in Fig. 10. The most pronounced oscillation is the one in the mid 1950's noticed by Favorite and McLain (1974), but three other oscillations are also clearly evident. The 1960's seem characterized by less well defined, longer period oscillations, than those in the 1950's, but the basic pattern is still recognizable. The period between peaks varies between five and seven years, so phase lag estimates made above are probably slightly too short and phase speeds slightly too fast.

5. Discussion

Full discussion of mechanisms behind the observed SST anomaly patterns must await results of a study of both SST and atmospheric pressure variance pat-

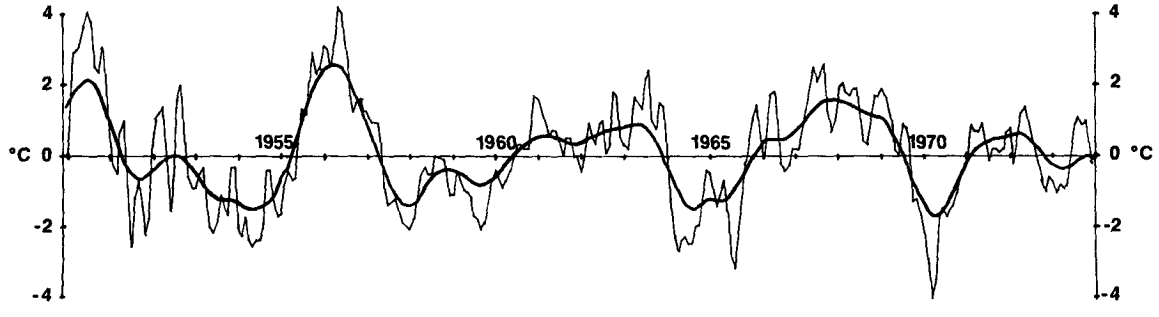

FIG. 10. Time series of first FDPC and smoothed version.

terns currently being undertaken by this author, but some suggestions can be advanced in light of existing literature. The question of mechanisms can be divided into two parts: First, what is causing anomalies to develop in the manner described? Second, why does a similar pattern develop roughly every four to seven years? In other words, what factors are involved in the evolution of SST anomalies in the midlatitude North Pacific as described above, and what is modulating the time scales on which these patterns seem to operate?

Taking the second question first, there is some evidence of oscillatory patterns on these time scales for a number of variables relating to atmospheric and oceanic circulation in the North Pacific region. Sea-level pressure (Wagner, 1971), California coastal SST's (Michaelsen, 1977), mid-Pacific blocking frequencies (White and Clark, 1975), and meridional baroclinic transport across the Subtropical gyre (White, 1975) all show strong variability on four to seven year time scales.

There are no indications from any of these studies or from the present study what mechanisms are responsible for modulating the oscillations. The hypothesis that anomalies continuously circle the subtropical gyre (Favorite and McLain, 1974) cannot be ruled out since the study area used in this paper does not include all of the gyre. The decrease in coherence during the eastward movement of the anomaly progression does raise strong doubts about the likelihood that the circuit is completed on a regular basis, however.

Returning to the first question, a possible explanation of the rapid expansion and intensification of SST anomalies in the western North Pacific can be found in an analytical modeling study by Pedlosky (1975). He postulated a positive feedback system consisting of interactions between the atmospheric long waves, baroclinic cyclone waves, and the SST field.

According to his model a small SST anomaly which intensifies the north–south oceanic temperature gradient acts to destabilize cyclonic waves by increasing the baroclinicity of the atmosphere. Potential vorticity transport by the cyclonic waves is balanced by vortex tube stretching driven by heat transfer from the ocean which is in turn balanced by meridional wind-driven advection of SST. This requires a change in the large-scale atmospheric thermal wind. The spatial phase of the advection is such that the SST anomaly intensifies, leading to greater destabilization of cyclonic waves. The eastward drift of the intensified SST anomalies may be produced by normal current movement, as well as anomalous wind drift. Observational evidence for the importance of both phenomena has been provided by Namias (1972).

Since cyclonic activity is a crucial component in this positive feedback system, it is evident that it could only be effective in areas statistically preferred for cyclonic activity. This could explain why intensification of the SST anomalies seems most pronounced in the region of the Kamchatka Trough. It could also explain why deterioration generally accompanies the eastward drift of the anomalies out of the region of strong cyclogenesis. Other factors could be the spatial inhomogeneity of the thermal connection between the two media (Namias, 1973) and negative feedbacks of the sort identified by Namias (1976).

6. Summary

Frequency domain principal components analysis has been presented as an alternative to standard principal components analysis for studying the variability of spatially arranged time series. FDPC analysis gives one the ability to identify features which migrate in space over time and to focus on specific time scales of interest.

The existence of coherent migrating SST anomalies in the North Pacific has been hypothesized by others and is verified to a certain extent by the findings presented above. The predominant feature of the low frequency SST field is seen to be a progression of anomalies out of the southwest North Pacific into the western half of the midlatitude North Pacific. In that region the anomalies tend to expand rapidly and intensify. They begin to drift eastward, but do not always remain sufficiently coherent to be identified at the eastern boundary of the ocean. The possibility of a continuous cycling of anomalies around the North Pacific gyre cannot be ruled out since much of the westward return flow would be out of the area analyzed here. The frequent deterioration of anomalies during their eastward passage in midlatitudes, however, puts this theory in serious doubt.

It is suggested that the rapid expansion and intensification of the SST anomalies in the western North Pacific results from a three-way positive feedback between the SST anomalies, baroclinic cyclone waves, and the long waves in the atmosphere. The findings of Davis (1976) indicate that during the period of maximum development of the SST anomalies the atmosphere tends to lead the ocean. It appears, however, that the SST anomalies have already been developing for about a year prior to this time. Thus, it does not necessarily follow that the atmosphere leads (and therefore forces) the ocean throughout the development of the SST anomalies. The return period of the anomalies varies between about four and seven years.

Acknowledgments. The author gratefully acknowledges the helpful comments of Drs. David Brillinger, Jerome Namias, and Orman Granger, as well as those of the two reviewers. Susan Chamberlin did the graphics and Natalia Vonnegut the typing.

REFERENCES

Brillinger, D. R., 1975: *Time Series Data Analysis and Theory.* Holt, Rinehart and Winston, 500 pp.

Davis, R. E., 1976: Predictability of sea surface temperature and sea level pressure anomalies over the North Pacific Ocean. *J. Phys. Oceanogr.*, **6,** 249–266.

Favorite, F., and D. R. McLain, 1974: Coherence in transPacific movements of positive and negative anomalies of sea surface temperature, 1953–60. *Nature*, **244,** 139–143.

Jenkins, G. M., and D. G. Watts, 1968: *Spectral Analysis and Its Applications.* Holden-Day, 525 pp.

Michaelsen, J., 1977: North Pacific sea surface temperatures and California precipitation. M.A. thesis, Dept. of Geography, University of California, Berkeley, 121 pp.

Namias, J., 1959: Recent seasonal interactions between North Pacific waters and the overlying atmospheric circulation. *J. Geophys. Res.*, **64,** 631–646.

——, 1969: Seasonal interactions between the North Pacific Ocean and the atmosphere during the 1960's. *Mon. Wea. Rev.*, **97,** 173–192.

——, 1970: Macroscale variations in sea-surface temperatures in the North Pacific. *J. Geophys. Res.*, **75,** 565–582.

——, 1972: Experiments in objectively predicting some atmospheric variables for the winter of 1971–72. *J. Appl. Meteor.*, **11,** 1164–1174.

——, 1973: Thermal communication between the sea surface and the lower troposphere. *J. Phys. Oceanogr.*, **3,** 373–378.

——, 1976: Negative ocean–air feedback systems over the North Pacific in the transition from warm to cold seasons. *Mon. Wea. Rev.*, **104,** 1107–1121.

Pedlosky, J., 1975: The development of thermal anomalies in a coupled ocean–atmosphere model. *J. Atmos. Sci.*, **32,** 1501–1514.

Wagner, A. J., 1971: Long period variations in seasonal sea level pressure over the Northern Hemisphere. *Mon. Wea. Rev.*, **99,** 49–66.

Wallace, J. M., 1972: Empirical orthogonal representation of time series in the frequency domain. *J. Appl. Meteor.*, **11,** 893–900.

——, and R. E. Dickinson, 1972: Empirical orthogonal representation of time series in the frequency domain. Part I: Theoretical considerations. *J. Appl. Meteor.*, **11,** 887–892.

Weare, B. C., A. R. Navato and R. E. Newell, 1976: Empirical orthogonal analysis of Pacific sea surface temperatures. *J. Phys. Oceanogr.*, **6,** 671–678.

White, W. B., 1975: Secular variability in the large-scale baroclinic transport of the North Pacific from 1950–1970. *J. Mar. Res.*, **33,** 144–155.

——, and N. E. Clark, 1975: On the development of blocking ridge activity over the central North Pacific. *J. Atmos. Sci.*, **32,** 489–502.